Energy & Environmental Science

RSC Publishing

PAPER

View Article Online
View Journal | View Issue

5.2% efficient PbS nanocrystal Schottky solar cells†

Cite this: *Energy Environ. Sci.*, 2013, **6**, 3054

Claudia Piliego,[a] Loredana Protesescu,[bc] Satria Zulkarnaen Bisri,[a] Maksym V. Kovalenko[bc] and Maria Antonietta Loi*[a]

Received 9th May 2013
Accepted 31st July 2013

DOI: 10.1039/c3ee41479e

www.rsc.org/ees

The impact of post-synthetic treatments of nanocrystals (NCs) on the performance of Schottky solar cells, where the active PbS nanocrystal layer is sandwiched directly between two electrodes, is investigated. By monitoring the amount of ligands on the surface of the nanocrystals through Fourier Transform Infrared (FTIR) measurements, we find that optimized processing conditions can lead to high current density and thus to an increase in overall efficiency. Our devices reach an efficiency of 5.2%, which is the highest reported using a PbS nanocrystal Schottky junction. These results demonstrate that even by using the simplest device architecture, accurate post-synthetic treatments result in substantial improvements in the performance. By drawing a direct correlation between ligand-to-NC ratio in the starting PbS solution and the device parameters, we provide important insights on how to gain experimental control for the fabrication of efficient PbS solar cells.

Broader context

The need for alternative energy sources is attracting both academic and industrial interest towards the exploration of novel approaches for fabrication of efficient, low-cost solar cells. Solution processed-colloidal nanocrystals (NCs) are one of the most promising candidates for the next generation photovoltaics. Highly efficient NC based solar cells can be fabricated on large areas at low cost. The quantum size effect in NCs and the resulting wide tunability allow for light harvesting spanning a broad range of the solar spectrum, including the near infrared. In this paper, high-efficiency NC solar cells are reported by using a simple device architecture, where the active layer is inserted directly between two electrodes. Through a systematic study on the post-synthetic procedure, we find a direct correlation between the NC properties in the starting solution and the resulting device performance. Our results provide important guidelines on how to gain experimental control on the fabrication of efficient NC solar cells.

Introduction

The need for alternative energy sources has recently increased the attention on nanomaterial based technologies.[1] Recent advances in the synthesis and the characterization of semiconductor nanocrystals (NCs) have greatly improved the ability to tailor their electronic and optical properties, making them suitable for several applications. In particular, lead chalcogenide nanocrystals show very strong quantum confinement[2] and broad-band absorption[3,4] that make them attractive for applications in photovoltaic (PV) cells,[5,6] photodetectors,[7,8] light-emitting diodes,[9,10] and thermoelectric devices.[11] Among this group of materials, PbS nanocrystals[12] have demonstrated very promising results in PV applications,[13] with several reports showing improvements on both device efficiency[14,15] and stability.[16,17] In order to increase the performance, PbS nanocrystals have been employed in complex device architectures, such as depleted heterojunction solar cells,[18] in inverted[19] or tandem configurations,[20] quantum junctions[21] obtained with two layers of PbS with different doping, and bilayered structures in combination with other nanocrystals.[22] Despite all the efforts in the engineering of the device structure, there is still a lack of knowledge regarding the properties of the nanocrystals in the starting solution with a direct impact on device performance. Some factors, which can be controlled during the synthesis such as fully passivated surfaces,[14] well-controlled size,[23,24] and narrow particle size distribution,[25] have been recognized as critical for achieving high-quality nanocrystals. However, the impact of other properties, such as the ratio in the starting solution between nanocrystals, ligands, and unintentional contaminants, is far less understood. To investigate the effect of these properties, we chose to use the Schottky architecture. Fabrication of solar cells using this structure is straightforward: PbS nanocrystals deposited onto indium tin oxide (ITO) form an ohmic contact, and thermally evaporated metal electrodes on top form the Schottky junction. Such a structure allows for a systematic investigation of the quality of the nanocrystals on the device performance, since PbS is the only photoactive and

[a]Zernike Institute for Advanced Materials, University of Groningen, Nijenborgh 4, Groningen, 9747 AG, The Netherlands. E-mail: m.a.loi@rug.nl
[b]Department of Chemistry and Applied Biosciences, ETH Zürich, Wolfgang-Pauli-Str. 10, Zurich, 8093, Switzerland
[c]EMPA-Swiss Federal Laboratories for Materials Science and Technology, Überlandstrasse 129, Dübendorf, 8600, Switzerland

† Electronic supplementary information (ESI) available. See DOI: 10.1039/c3ee41479e

conductive material. Early devices made with this structure typically resulted in a solar power conversion efficiency around 2%.[26,27] Recent demonstrations of improved efficiency[28] and stability[29] motivate the selection of this structure for our study. Moreover, the absence of any additional layer greatly decreases the manufacturing costs and avoids additional interfaces that can be detrimental to device stability.[30,31]

The as-synthesized nanocrystals are dispersed in a mixture of solvents (in our samples oleic acid (OA) and 1-octadecene (ODE)). The process to remove nanocrystals from the synthesis mixture and to re-disperse them in a solvent suitable for device fabrication, such as toluene or chloroform, is referred to as the "cleaning process". The procedure consists of adding a non-solvent, a mixture of ethanol and hexane to precipitate the nanocrystals and to remove the initial solvent along with unreacted precursors and byproducts. The process has been repeated several times (namely *PbS_3 washing steps*, *PbS_4 washing steps* and *PbS_5 washing steps*) before dissolving the nanocrystals in chloroform. Despite the importance of this procedure, at the best of our knowledge, a systematic study correlating the ligand-to-NC ratio to the device performance is still missing. In this paper, we fill this gap by showing a direct correlation between the amount of capping ligands on the NC surface and the PV device parameters. The amount of ligands is controlled by the number of washing steps of the starting PbS solution. We are able to determine the optimal conditions, identifying also a limit for this procedure. Our devices yielded a record efficiency of 5.2% under simulated AM 1.5 illumination, which is the highest efficiency reported for PbS solar cells using a Schottky junction.

Results and discussion

For this study, we selected PbS NCs with the first excitonic peak at $\lambda \approx 1100$ nm (3.7 nm) (Fig. 1). After the synthesis, the washing procedure was carried out as follows: hexane (40 mL) and ethanol (80 mL) were added to the crude solution followed by centrifugation to separate NCs. The PbS NCs were then re-dispersed in hexane (40 mL) and precipitated again with ethanol (35 mL). After another washing cycle with ethanol/hexane, the particles were re-dispersed in chloroform (12 mL) (*PbS_3 washing steps*). A part of this solution was further precipitated from chloroform with methanol and re-dispersed in chloroform (*PbS_4 washing steps*). In search of the optimal conditions for the cleaning procedure an extra washing step with chloroform and methanol was performed (*PbS_5 washing steps*).

Fig. 2 presents typical Fourier Transform Infrared (FTIR) spectra of the PbS nanocrystal films drop-cast from the solutions that have undergone different cleaning treatments. From these spectra it is possible to detect the chemical species present on the surface of the PbS NCs and eventual impurities. From the C–H stretching mode region shown in Fig. 2a, we estimate the amount of capping ligands on the surface of the particles. The peaks at 2921 cm^{-1}, 2917 cm^{-1}, 2904 cm^{-1} (shoulder) and 2853 cm^{-1} are assigned to anti-symmetric and symmetric methylene stretch modes ($\nu_{(as)}CH_2$, $\nu_{(s)}CH_2$)[32,33] (see Fig. S1†) and the peak at 1952 cm^{-1} is characteristic of the

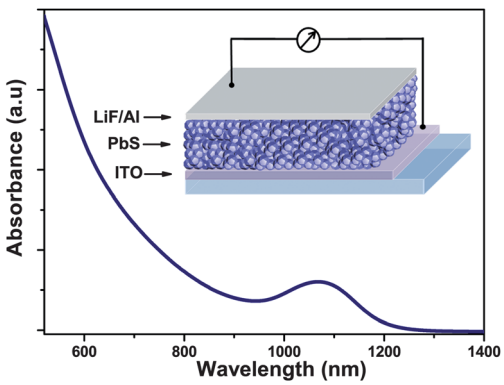

Fig. 1 (a) Absorption spectrum of oleic acid (OA) capped PbS nanocrystals dispersed in chloroform. Inset: the schematic of the photovoltaic device structure with the nanocrystal layer inserted between the ITO and the LiF/Al electrode.

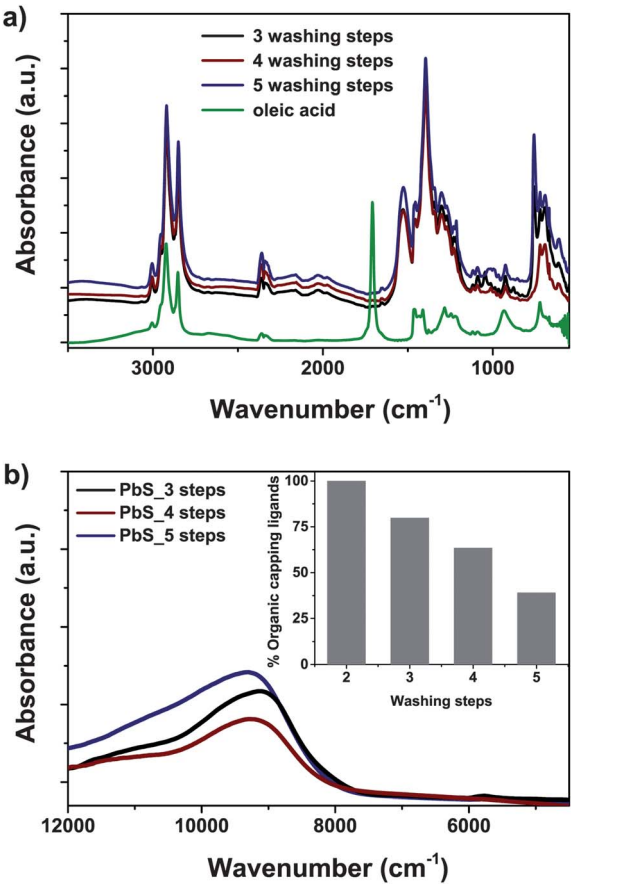

Fig. 2 (a) FTIR C–H stretching region for different washing steps: the peaks at 2921 cm^{-1}, 2917 cm^{-1}, 2904 cm^{-1} and 2853 cm^{-1} are assigned to antisymmetric and symmetric methylene stretch modes ($\nu_{(as)}CH_2$, $\nu_{(s)}CH_2$); the peak at 1952 cm^{-1} characterizes the asymmetric methyl stretching ($\nu_{(as)}CH_3$) of oleic acid molecules. The green line represents the spectrum of the free oleic acid and the peak at 1708 cm^{-1} corresponds to the C=O stretching of carboxylate in acidic form. (b) FTIR spectra of PbS nanocrystals coated with oleic acid with the first excitation peak at 9270 cm^{-1}. Inset: ratio between the integrated area of the PbS peak and the C–H stretching vibrations measured on films obtained from solutions with different washing steps.

asymmetric methyl stretching ($\nu_{(as)}CH_3$)[32] in oleic acid molecules. The integration of the area underneath these peaks gives an estimation of the amount of oleic acid present on the surface of the nanocrystals. Moreover, the absence of the peak corresponding to C=O stretching of carboxylate in acidic form (1708 cm^{-1}),[34] which can be observed in the oleic acid spectrum (the green line in Fig. 2a), leads to the conclusion that there are no free ligands in the PbS colloidal films regardless of the number of washing steps of the solutions. Fig. 2b shows the excitonic peak of the PbS particles at 9270 cm^{-1} (1078 nm). The position of the peak is nearly identical for all samples, indicating that the average NC size is not affected by the number of washing steps. The position and separation of the $\nu(COO^-)$ band, Δ, in the 1700–1300 cm^{-1} region can be used to deduce the carboxylate coordination mode.[33–37] For PbS capped NCs we observe that the wavenumber separation between $\nu_{(as)}(COO^-)$ 1526 cm^{-1} and $\nu_{(s)}(COO^-)$ 1396 cm^{-1} is 130 cm^{-1} and it can be assigned to a bidentate coordination[35,38] (Fig. S2†). Another long hydrocarbon chain compound like octadecene (Fig. S3†) is most likely absent from the washed PbS solution because the ratio between the intensity of ν(CH) and $\nu(COO^-)$ is relatively low while in the octadecene infrared spectrum the ν(C=C) peak is considerably weaker than CH asymmetric and symmetric vibration peaks. Moreover, the spectrum for PbS solution washed 4 times does not show the characteristic peak for ν(C=C) vibration at 1641 cm^{-1} (Fig. S3†). The degree of surface oxidation, which would have shifted the peak to shorter wavelengths, is negligible as well. From the comparison of the integrated area corresponding to the PbS peak (9270 cm^{-1}) and to C–H stretching vibration (2921–2853 cm^{-1}) we can estimate the decrease of the oleic acid content on the surface of NCs, following each washing step (the inset of Fig. 2b). We observe a significant difference (16.4%) between the sample with 3 regular washing steps (*PbS_3 washing steps*) with ethanol/hexane and the sample that undergoes one additional washing cycle with methanol/chloroform (*PbS_4 washing steps*). An extra washing step (*PbS_5 washing steps*) further decreases the concentration of capping oleate. As a consequence, the solubility of the particles in chloroform becomes significantly lower. Further washing would reduce the solubility even more, making the PbS nanocrystals unsuitable for device fabrication. From all these observations, we can conclude that the number of washing steps is primarily affecting the amount of ligands attached to the nanocrystal surface. In order to obtain efficient solar cells an optimal balance has to be achieved in the ligand-to-NC ratio, which guarantees sufficiently good solubility for the processing without affecting the device performance due to trapping and hindering of the carrier transport.

To determine the optimal conditions for the post-synthetic processing, we fabricated solar cells with the different PbS solutions, adopting the simple Schottky layout shown in the inset of Fig. 1a. A thin layer of PbS–OA in chloroform solution was deposited on top of the ITO substrate by spin-coating, followed by the ligand exchange treatment. The ligand exchange was carried out by casting 1,4-benzenedithiol (BDT) solution in acetonitrile (AcCN) on top of the PbS–OA blend film: after waiting for a few seconds for the exchange reaction to take place, the substrate was spin-coated at high speed to remove the solvent. Short bidentate ligands, such as BDT, effectively replace the long insulating chains and reduce the inter-particle spacing. This leads to increased electronic coupling between NCs and to crosslinking of the thin layer. The BDT treatment has been reported to be less aggressive than 1,2 ethanedithiol (EDT) treatment,[39] leading to lower trap density[40] and improved device performance and stability.[41] For these reasons we selected this ligand, but we expect the results to be independent of the specific ligand exchange treatment.

The two-step deposition was repeated several times in order to obtain a uniform and crack-free film, having an optimal thickness of 140–150 nm. After annealing at 140 °C for 10 minutes, the device fabrication was completed by the thermal evaporation of an electrode consisting of 100 nm Al on top of ~1 nm LiF. More than 30 devices have been fabricated for every washing condition (~90 devices in total) using different batches of PbS nanocrystals, in order to test the result reproducibility. The current–voltage characteristics of the best devices under simulated AM 1.5 test conditions are plotted in Fig. 3 and the corresponding parameters are reported in Table 1, together with the average values. During the fabrication of the devices, we kept the conditions for the BDT treatment constant. We assume that the ligand exchange process is equally effective on the nanocrystal films, irrespective of the amount of ligands present on the surface that is changing with the number of

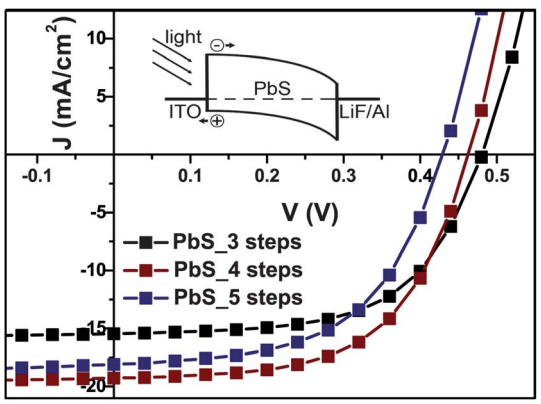

Fig. 3 Current density–voltage characteristics (*J–V*) of devices fabricated using the PbS solution washed 3, 4 and 5 times. Inset: the diagram of the energy levels of the junction under illumination.

Table 1 Parameters of the best performing devices, as a function of the number of washing steps. The average values (of all devices) are reported in the round brackets

	J_{sc} (mA cm^{-2})	V_{oc} (V)	FF (%)	PCE (%)	R_S (Ω cm^2)	R_{SH} (kΩ cm^2)
PbS	−15.4	0.48	59	4.4	28	18.0
3_washing	(−15)	(0.478)	(58.5)	(4.2)		
PbS	−19.3	0.46	58	5.2	24	15.3
4_washing	(−18.5)	(0.46)	(57)	(4.9)		
PbS	−18.0	0.43	55	4.3	27	8.2
5_washing	(−17)	(0.43)	(54)	(4)		

washing steps. This assumption is supported by previous data[28] and by the observation that films spin-coated from the solutions with different cleaning steps (*PbS_3 washing steps*, *PbS_4 washing steps*, *PbS_5 washing steps*) provided smooth layers of identical thickness.

In devices fabricated with the solution that underwent 4 washing steps (*PbS_4 washing steps*), we observe an increase in the photocurrent and a decrease in the open circuit voltage with respect to devices from solutions with 3 washing steps (*PbS_3 washing steps*) (Fig. 3). In particular, the best device from *PbS_4 washing steps* showed a power conversion efficiency of 5.2% with a J_{sc} of 19.3 mA cm^{-2} and a V_{oc} of 0.46 V (Fig. 4a). In order to quantify the optimal number of washing steps, we added an extra step, by performing the cleaning with chloroform and methanol twice, before drying the NCs and re-dispersing them in anhydrous chloroform for the device fabrication. However, the devices prepared using this solution, *PbS_5 washing steps*, showed a reduction in both the J_{sc} and the V_{oc} (Fig. 3), leading to a lower PCE. Clearly, the best procedure consists of 4 washing steps: irrespective of the specific post-synthesis treatment, these results give us an indication of the optimal ligand-to-NC ratio (see inset Fig. 2b), able to provide a remarkable device performance, mostly due to an increase in the photocurrent. The external quantum efficiency (EQE) spectrum of one of the best devices is shown in Fig. 4b.

To understand how the different ligand-to-NC ratios are affecting the device performance, we examined the values of the series resistance (R_S) and the shunt resistance (R_{SH}) (Table 1) of each device. R_S is related to the intrinsic resistance of the NC layer and the resistance at the contacts. The finite value of R_{SH} is associated with the presence of current leakage paths through the solar cell and recombination of charge carriers. The higher value of photocurrent and the resulting higher efficiency in devices from *PbS_4 washing steps* with respect to devices from *PbS_3 washing steps* is due to the improved transport in the film, as shown by the lower series resistance. The presence of fewer insulating ligands on the surface of the NCs, when they are in solution, translates into a better connectivity and into a reduced resistance in the film after they undergo the ligand exchange treatment. This explanation is also supported by the current–voltage characteristics of field-effect transistors realized from the same solutions and following the same procedure as the solar cells. Devices from *PbS_4 washing steps* show higher electron current with respect to devices from *PbS_3 washing steps* (see Fig. S4†).

On the other hand, the slightly lower value of R_{SH} in the devices from *PbS_4 washing steps* is an indication of charge recombination. Due to the reduced coverage of the nanocrystal surface by oleic acid in *PbS_4 washing steps* with respect to *PbS_3 washing steps*, the ligand exchange process results in a less passivated surface. This hypothesis is confirmed by the even lower value of R_{SH} in the devices from *PbS_5 washing steps*. The increased interfacial recombination due to the increase in the number of washing steps is a possible explanation of the decreasing trend in V_{oc} observed in these devices. Despite the difficulties in quantifying the V_{oc} in NC based solar cells, due to the challenges in positioning the energy levels, a device that can build up a larger quantity of separated charges would generally yield a higher V_{oc}. We conclude that the lower passivation of the NC surface increases the recombination of charges, which ultimately lowers the V_{oc} in the devices from *PbS_4* and *PbS_5 washing steps.*

Therefore in *PbS_4 washing steps*, the optimal balance has been achieved between the solubility and purity of the nanocrystals, while maintaining sufficient electronic passivation. Any additional washing step, as shown by *PbS_5 washing steps*, is not beneficial. Excessive washing probably damages the surface of the nanocrystals and may alter the Pb-to-S atomic ratio (if oleate is removed in the form of lead oleate). Moreover the reduced number of ligands decreases the solubility of the nanocrystals, which ultimately affects the processability and the quality of the film.

Since the post-synthesis procedure affects the surface of the nanocrystals, it is more critical for small nanocrystals.[42] However, it still has an influence on NCs of bigger size.

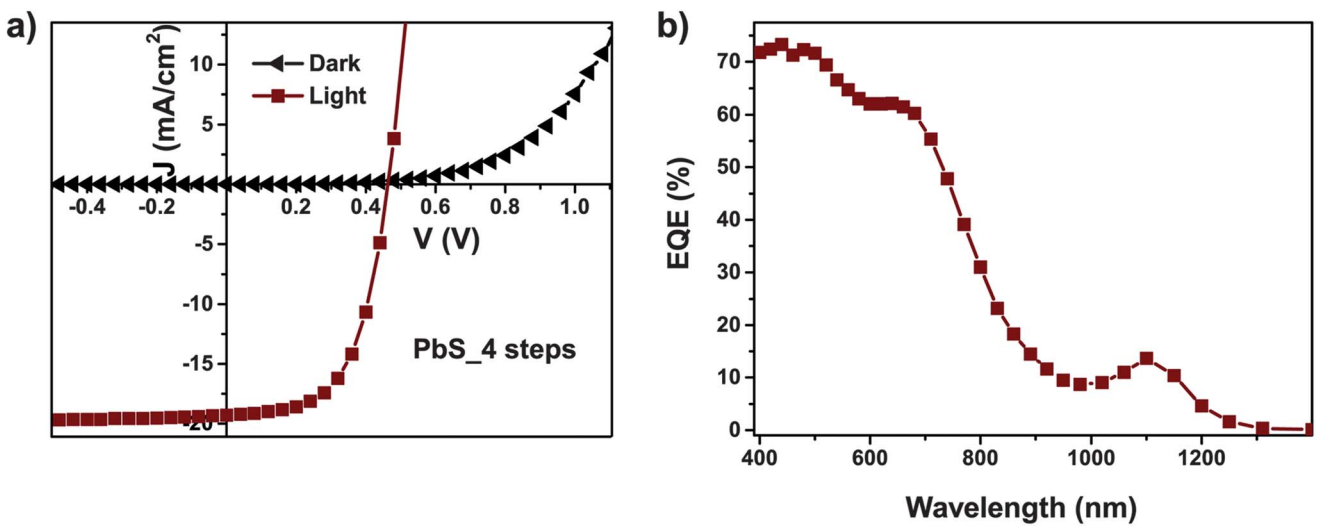

Fig. 4 (a) Current–voltage characteristics in the dark and under 100 mW cm^{-2} AM 1.5 illumination of the best device realized with *PbS_4 washing step* solution. (b) External quantum efficiency spectrum (EQE) of the same device.

The same study performed on larger PbS nanocrystals ($\lambda \approx 1270$ nm, 4.5 nm) provided similar results. We observed an increase of the J_{sc} and a decrease of the V_{oc} for *PbS_4 washing steps* with respect to *PbS_3 washing steps*. Despite the difference in current and efficiency being less striking (see Fig. S5 and S6†), these results show a general trend in the PV parameters as a function of the ligand-to-NC ratio.

In conclusion, we report a systematic study on the impact of the post-synthetic procedure on PbS photovoltaic performance. We find a direct correlation between the amount of capping ligands on the surface of the nanocrystals in the starting solution and the efficiency parameters in solar cells. By optimizing the process a PCE of 5.2% is achieved. This is the highest efficiency reported, to the best of our knowledge, using the simple Schottky junction with the PbS nanocrystals layer sandwiched between two electrodes. The striking results obtained, using such a basic device configuration, underline the very sensitive relationship between the properties of the nanocrystals in the starting solution and the resulting device performance. Our work aims at providing guidelines for the post-synthesis treatment of PbS nanocrystals, with the objective to successfully translate the promising device performance reported for PbS solar cells into a technological reality in the near future.

Experimental

Materials

PbS nanocrystal synthesis. In a three-neck reaction flask, $PbAc_2 \times 3H_2O$ (4 mmol, 1.5 g), ODE (50 mL) and OA (4.5 mL) were dried at 120 °C under vacuum for 2 hours to dissolve lead salt and to dry the solution. The temperature was raised to 145 °C. In a glovebox, sulfur precursor solution was prepared by mixing TMS_2S (0.42 mL, 2 mmol) with ODE (10 mL). Sulfur solution was quickly injected into the reaction flask at 145 °C followed by the removal of the heating mantle for 3 minutes and cooling to room temperature using a water bath. The washing procedure was carried out in air. Hexane (40 mL) and ethanol (80 mL) were added to the crude solution followed by centrifugation to separate NCs. The obtained PbS NCs were re-dispersed in hexane (40 mL), and precipitated again with ethanol (35 mL). After one more washing step with ethanol/hexane, the particles were re-dispersed in chloroform (12 mL), to obtain samples with 3 washing steps. For 4 washing steps samples, the particles were further precipitated from chloroform with methanol and re-dispersed in chloroform. For 5 washing steps samples the procedure as in the 4 washing steps was further repeated.

Infrared spectroscopy

The infrared spectra for the 14 000–2000 cm^{-1} range were collected with a Vertex 80 Spectrometer with a HATR accessory and a ZnSe crystal using a DLaTGS-KBr detector with a CaF_2 beam splitter. The spectra were acquired using 32 scans. For mid-FTIR spectra (4000–800 cm^{-1}), a Nicolet iS5 spectrometer with a DTGS-KBr detector and a KBr beamsplitter with an ATR accessory and a diamond crystal were used. The samples were prepared by evaporating the chloroform solution of PbS nanocrystals on a Si/SiO_2 substrate. The spectra were collected using 32 scans from which a background spectrum of the substrate was automatically extracted. Measurements were repeated several times to check reproducibility.

Device characterization

Solar cells. Current–voltage characteristics were recorded using a Keithley 2400 Source Meter with the device kept in a nitrogen-filled glove box. Measurements were performed in the dark and under illumination from a Steuernagel Solar Constant 1200 metal halide lamp calibrated to 1 sun intensity and corrected for spectral mismatch with an AM 1.5G spectrum using a Si reference cell. Contributions to the photocurrent from regions outside the anode/cathode overlap area were eliminated using a mask with a slightly smaller aperture than the device area. External quantum efficiency (EQE) spectra were measured from 400 nm to 1400 nm using a custom-built set-up consisting of a 50 W quartz tungsten halogen lamp (Newport research series) with a highly stable radiometric power supply, 33 narrow band-pass filters (CVI laser), a trans-impedance amplifier and a Stanford Research System SR830 lock-in amplifier. The spectral response was measured relative to that of a calibrated Si (Newport 818-SL) and a Ge (Oriel 71653) photodiode.

Calculation of R_S and R_{SH}

The series resistance R_S under illumination was estimated by a comparison of the *I–V* characteristics of PV devices in the dark and under illumination using the following equation, as from the simple model reported in the literature[43,44]

$$R_S = \frac{V_{dark,mpp} - V_{ligth,mpp} - \left(|J_{SC}| - |J_{mpp}|\right) R_{S,dark}}{|J_{mpp}|}$$

where the index mpp is the maximum power point and the light and dark indicates the characteristics taken under illumination and in the dark, respectively. $R_{S,dark}$ is the dark series resistance, which is given by

$$R_{S,dark} = \frac{V_{dark,J_{sc}} - V_{oc}}{|J_{sc}|}$$

The parallel resistance R_{SH} in the dark was obtained by applying Ohm's law, using the inverse slope of the linear fit between −0.1 V and 0.1 V in the *I–V* characteristics.

Transistor measurements were performed using a probe station inside a nitrogen-filled glovebox under dark conditions at room temperature. The transistor characteristics were acquired using an Agilent E5270B semiconductor parameter analyzer.

Layer thickness measurements were performed using a Veeco Dektak 6M profilometer. Absorption spectra were recorded using a Perkin Elmer lambda 900 spectrometer.

Acknowledgements

Financial support from the European Research Council ("HySPOD" ERC StG 306983) and the Zernike Institute for Advanced

Materials is gratefully acknowledged. The authors thank J. Harkema, R. Gooijaarts and A. Kamp for technical support. D. Norris and M. Heinrich are acknowledged for the use of their Vertex FTIR spectrometer.

References

1 D. V. Talapin, J.-S. Lee, M. V. Kovalenko and E. V. Shevchenko, *Chem. Rev.*, 2010, **110**, 389–458.
2 F. W. Wise, *Acc. Chem. Res.*, 2000, **33**, 773–780.
3 H. Du, C. Chen, R. Krishnan, T. D. Krauss, J. M. Harbold, F. W. Wise, M. G. Thomas and J. Silcox, *Nano Lett.*, 2002, **22**, 1321–1324.
4 C. M. Evans, L. Guo, J. J. Peterson, S. Maccagnano-Zacher and T. D. Krauss, *Nano Lett.*, 2008, **8**, 2896–2899.
5 W. Ma, J. M. Luther, H. Zheng, Y. Wu and A. P. Alivisatos, *Nano Lett.*, 2009, **9**, 1699–1703.
6 W. Ma, S. L. Swisher, T. Ewers, J. Engel, V. E. Ferry, H. Atwater and A. P. Alivisatos, *ACS Nano*, 2011, **5**, 8140–8147.
7 K. Szendrei, F. Cordella, M. V. Kovalenko, M. Yarema, D. Jarzab, O. V. Mikhnenko, P. W. Blom, W. Heiss and M. A. Loi, *Adv. Mater.*, 2009, **21**, 683–687.
8 G. Konstantatos, I. Howard, A. Fischer, S. Hoogland, J. Clifford, E. Klem, L. Levina and E. H. Sargent, *Nature*, 2006, **442**, 180–183.
9 J. S. Steckel, S. Coe-Sullivan, V. Bulović and M. G. Bawendi, *Adv. Mater.*, 2003, **15**, 1862–1866.
10 L. Sun, J. J. Choi, D. Stachnik, A. C. Bartnik, B.-R. Hyun, G. G. Malliaras, T. Hanrath and F. W. Wise, *Nat. Nanotechnol.*, 2012, **7**, 369–373.
11 R. Y. Wang, J. P. Feser, J.-S. Lee, D. V. Talapin, R. Segalman and A. Majumdar, *Nano Lett.*, 2008, **8**, 2283–2288.
12 J. Tang and E. H. Sargent, *Adv. Mater.*, 2011, **23**, 12–29.
13 I. J. Kramer and E. H. Sargent, *ACS Nano*, 2011, **5**, 8506–8514.
14 J. Tang, K. W. Kemp, S. Hoogland, K. S. Jeong, H. Liu, L. Levina, M. Furukawa, X. Wang, R. Debnath, D. Cha, K. W. Chou, A. Fischer, A. Amassian, J. B. Asbury and E. H. Sargent, *Nat. Mater.*, 2011, **10**, 765–771.
15 D. A. R. Barkhouse, R. Debnath, I. J. Kramer, D. Zhitomirsky, A. G. Pattantyus-Abraham, L. Levina, L. Etgar, M. Grätzel and E. H. Sargent, *Adv. Mater.*, 2011, **23**, 3134–3138.
16 I. J. Kramer, R. Debnath, G. I. Koleilat, X. Wang, A. Fisher, R. Li, L. Brzozowski, L. Levina and E. H. Sargent, *Adv. Mater.*, 2011, **23**, 3832–3837.
17 J. M. Luther, J. Gao, M. T. Lloyd, O. E. Semonin, M. C. Beard and A. J. Nozik, *Adv. Mater.*, 2010, **22**, 3704–3707.
18 A. G. Pattantyus-Abraham, I. J. Kramer, A. R. Barkhouse, X. Wang, G. Konstantatos, R. Debnath, L. Levina, I. Raabe, M. K. Nazeeruddin, M. Grätzel and E. H. Sargent, *ACS Nano*, 2011, **4**, 3374–3380.
19 J. Gao, J. M. Luther, O. E. Semonin, R. J. Ellingson, A. J. Nozik and M. C. Beard, *Nano Lett.*, 2011, **11**, 1002–1008.
20 X. Wang, G. I. Koleilat, J. Tang, H. Liu, I. J. Kramer, R. Debnath, L. Brzozowski, D. A. R. Barkhouse, L. Levina, S. Hoogland and E. H. Sargent, *Nat. Photonics*, 2011, **5**, 480–484.
21 J. Tang, H. Liu, D. Zhitomirsky, S. Hoogland, X. Wang, M. Furukawa, L. Levina and E. H. Sargent, *Nano Lett.*, 2012, **12**, 4889–4894.
22 A. K. Rath, M. Bernechea, L. Martinez, F. Pelayo Garcia de Arquer, J. Osmond and G. Konstantatos, *Nat. Photonics*, 2012, **6**, 529–534.
23 I. Moreels, K. Lambert, D. Smeets, D. De Muynck, T. Nollet, J. C. Martins, F. Vanhaecke, A. Vantomme, C. Delerue, G. Allan and Z. Hens, *ACS Nano*, 2009, **3**, 3023–3030.
24 D. Segets, J. M. Lucas, R. N. Klupp Taylor, M. Scheele, H. Zheng, A. P. Alivisatos and W. Peukert, *ACS Nano*, 2012, **6**, 9021–9032.
25 H. Fu, S.-W. Tsang, Y. Zhang, J. Ouyang, J. Lu, K. Yu and Y. Tao, *Chem. Mater.*, 2011, **23**, 1805–1810.
26 J. M. Luther, M. Law, M. C. Beard, Q. Song, M. O. Reese, R. J. Ellingson and A. J. Nozik, *Nano Lett.*, 2008, **8**, 3488–3492.
27 J. Tang, X. Wang, L. Brzozowski, D. A. R. Barkhouse, R. Debnath, L. Levina and E. H. Sargent, *Adv. Mater.*, 2010, **22**, 1398–1402.
28 K. Szendrei, W. Gomulya, M. Yarema, W. Heiss and M. A. Loi, *Appl. Phys. Lett.*, 2010, **97**, 203501.
29 K. Szendrei, Charge extraction from colloidal in organic nanocrystals, PhD thesis, University of Groningen, July 2011.
30 Z. B. Wang, M. G. Helander, J. Qiu, Z. W. Liu, M. T. Greiner and Z. H. Lu, *J. Appl. Phys.*, 2010, **108**, 024510.
31 M. G. Helander, Z. B. Wang, J. Qiu, M. T. Greiner, D. P. Puzzo, Z. W. Liu and Z. H. Lu, *Science*, 2011, **332**, 944–947.
32 M. J. Hostetler, J. J. Stokes and R. W. Murray, *Langmuir*, 1996, **12**, 3604–3612.
33 J. Huang, M. V. Kovalenko and D. V. Talapin, *J. Am. Chem. Soc.*, 2010, **132**, 15866–15868.
34 Y. Q. Lu and J. D. Miller, *J. Colloid Interface Sci.*, 2002, **256**, 41–52.
35 H. B. Abrahamson and H. C. Lukaski, *J. Inorg. Biochem.*, 1994, **54**, 115–130.
36 L. M. Bronstein, X. Huang, J. Retrum, A. Schmucker, M. Pink, B. D. Stein and B. Dragnea, *Chem. Mater.*, 2007, **19**, 3624–3632.
37 F. Soderlind, H. Pedersen, R. M. Petoral, P.-O. Kall and K. Uvdal, *J. Colloid Interface Sci.*, 2005, **288**, 140–148.
38 T. Bala, B. L. V. Prasad, M. Sastry, M. U. Kahaly and U. V. Waghmare, *J. Phys. Chem. A*, 2007, **111**, 6183–6190.
39 G. Sarasqueta, K. R. Choudhury and F. So, *Chem. Mater.*, 2010, **22**, 3496–3501.
40 K. Szendrei, M. Speirs, W. Gomulya, D. Jarzab, M. Manca, O. V. Mikhnenko, M. Yarema, B. J. Kooi, W. Heiss and M. A. Loi, *Adv. Funct. Mater.*, 2012, **22**, 1598–1605.
41 G. I. Koleilat, L. Levina, H. Shukla, S. H. Myrskog, S. Hinds, A. G. Pattantyus-Abraham and E. H. Sargent, *ACS Nano*, 2008, **2**, 833–840.
42 M. Soreni-Harari, N. Yaacobi-Gross, D. Steiner, A. Aharoni, U. Banin, O. Millo and N. Tessler, *Nano Lett.*, 2008, **8**, 678–684.
43 D. Pysch, A. Mette and S. W. Glunz, *Sol. Energy Mater. Sol. Cells*, 2007, **91**, 1698–1706.
44 K. F. Jeltsch, M. Schädel, J.-B. Bonekamp, P. Niyamakom, F. Rauscher, H. W. A. Lademann, I. Dumsch, S. Allard, U. Scherf and K. Meerholz, *Adv. Funct. Mater.*, 2011, **22**, 397–404.